A New Metallic Silicon Allotrope: c-Si16

X. Xie[a], Q. Wei[a,*], X. Jia[a],
Z. Wu[a] and M. Zhang[b]

[a] *School of Physics, Xidian University, Xi'an 710071, China*
[b] *College of Physics and Optoelectronic Technology, Baoji University of Arts and Sciences, 721016 Baoji, China*

Received: 06.02.2023 & Accepted: 28.08.2023

Doi: 10.12693/APhysPolA.144.173 *e-mail: qunwei@xidian.edu.cn

Using the structure search method combined with first-principles calculations, a new silicon allotrope with cubic symmetry, c-Si16, is proposed. To examine the stability of c-Si16 under ambient pressure, systematic calculations of its structural, mechanical, and electronic properties were performed. Mechanical and dynamic stability are demonstrated by elastic constants and phonon spectra, respectively. In addition, the band structure and density of states show that c-Si16 is a metallic silicon material, and its conductivity mainly comes from the p-orbital electrons of silicon.

topics: silicon, first-principles calculations, mechanical and electronic properties

1. Introduction

As the most abundant element on earth after oxygen, silicon has always been an important material for modern scientific and technological life in integrated circuits [1, 2], solar cells [3, 4], and the electrochemical industry. Scientists have been exploring to find silicon materials with better performance that could meet the development needs of the times. Due to the indirect band gap of conventional diamond-like silicon (DC-Si or Si-I) semiconductors, their application in light absorption is limited. This encourages us to make more experimental and theoretical innovations to search for more semiconductor materials with direct band gaps. The silicon allotrope offers us the possibility of further exploration. A complex free-energy landscape exists in silicon with abundant local minima [5]. As a result, this leads to the silicon structure having as many allotropes as carbon. By controlling the difference in decompression rate, we can obtain silicon allotropes with different structures and properties (Si-II, Si-XI, Si-V, Si-VI, Si-VII, Si-X phase [6–10]), and, as the pressure increases, the silicon coordination number will also increase, resulting in electron delocalization and increased metal abundance [11]. Therefore, this will cause all these silicon allotropes to exhibit metallic properties at specific temperatures and pressures, and once these conditions change a little, this stable state will no longer be maintained. Also, a reversible phase transition occurs under reduced pressure as well. It is worth noting that Si-I can be directly converted to Si-II, but Si-II cannot be directly converted to Si-I. If you want to get Si-I through Si-II, it requires multiple processes and phase transitions (Si-II → Si-XII → Si-III → Si-IV → Si-I) [11]. Since there is a large potential barrier in the transition from the high-pressure phase to the most stable Si-I phase at ambient temperature [12], the product after pressure relief is not the Si-I phase, but some metastable phases of silicon, such as Si-III, Si-XII, Si-IV [13, 14]. In addition, there is a large number of theoretically predicted different types and properties of silicon metastable phases [15–21] to address the growing demand for silicon materials with more abundant functions. Due to the different forms of silicon under normal pressure, we can try to continuously change the crystal structure of silicon to achieve different physical properties of silicon so as to seek a wider range of applications.

At present, most of the new structure predictions of silicon focus on semiconductor silicon, which can be divided into two categories. One is the silicon structure with a direct band gap, such as $P213$ phase [20], $oF16$-Si, $tP16$-Si, $mC12$-Si, and $tI16$-Si [21]. The other is the new structure with an indirect band gap, such as M phase, Z phase [22], Bct-Si [23], $M4$ phase [24], $T12$ phase [17], $st12$ phase [25], $C2/m$-16 phase, $C2/m$-20 phase, $Amm2$ phase, I-4 phase [26], and Si_{10} [27]. There are few reports on the structure of silicon with metallic properties. At present, only $hP12$-Si and m-Si_{20} with tunnel type are predicted by Sun [28] and Wang [29], but the higher overall energy of the latter brings some difficulties to further experimental

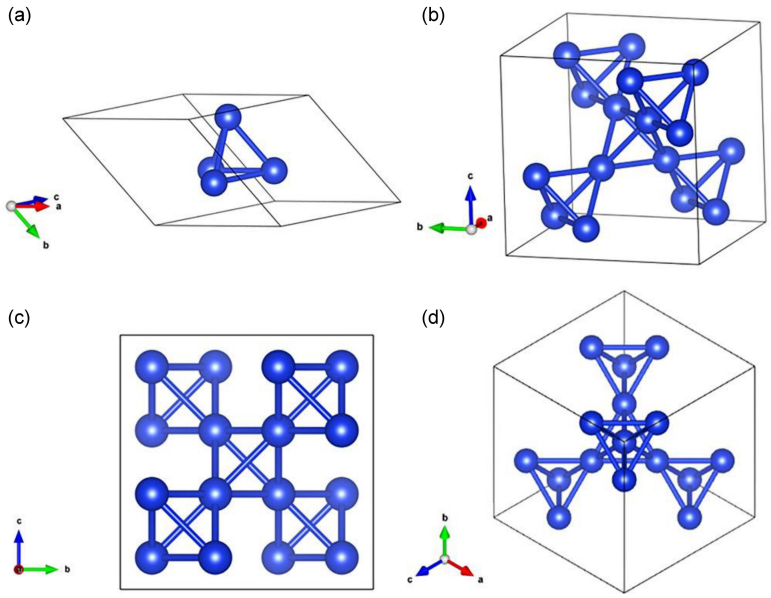

Fig. 1. (a) Primitive cell of *c*-Si16. (b) Conventional cell of *c*-Si16. (c) The crystal structure of *c*-Si16 viewed along the [100] direction. (d) The crystal structure of *c*-Si16 viewed along the [111] direction.

exploration. In addition, the characteristic that silicon easily reacts with metal to form metal silicide is also utilized, and then metal atoms are separated from the silicide to obtain silicon allotrope. For example, Sung et al. [30] predicted a new structure, $P6/m$-Si_6, the idea of which is to separate sodium atoms from the precursor of $P6/m$-$NaSi_6$ with an open frame and obtain silicon allotrope with superconducting properties. In 2013, Wen et al. [31] also adopted a similar approach to obtain tunnel-type quasi-direct band gap allotrope Si_{24} from Na_4Si_{24}.

In this work, a new metallic silicon allotrope was obtained for the first time through the crystal structure prediction technology. Through comparison with other silicon allotropes, the stability of this structure has been preliminarily verified. To further investigate the properties of various aspects of *c*-Si16, we calculated and analyzed the mechanical properties, band structure, and the electronic properties from first principles.

2. Computational method

The search for crystal structure was implemented in the CALYPSO code based on the global minimization of the energy surface and the *ab initio* total energy calculation [32, 33]. The recently published literature cases of successful application of this approach to structure prediction effectively illustrate the reliability of this approach [34–37]. In the initialization parameter setting of the crystal structure search, each formula unit was set with 16 atoms. During the structure evolution process, the global particle swarm optimization algorithm was used to conduct 30 generations of search, and each generation generated 30 structures. The relaxation of the structure was performed in the Vienna *Ab initio* Simulation Package (VASP) [38] using the generalized gradient approximation (GGA) exchange–correlation functional proposed by Perdew–Burke–Ernzerhof (PBE) [39] within the framework of density functional theory (DFT) [40]. The expanded basis set of the electronic wave function selects a plane wave, and the cut-off energy is determined to be 600 eV after the convergence test. In the Brillouin zone, the Monkhorst–Pack method was used to automatically generate k-points with the Γ-point as the center, and the k-point meshes were set to $5 \times 5 \times 5$ to complete the sampling to ensure that the convergence of the total energy was better than 1×10^{-5} eV/atom. Utilizing the force constant matrix obtained by VASP, the phonon dispersion spectrum is obtained by the density functional perturbation method combined with a supercell approach and Phonopy code [41]. The implementation of the PBE method enabled the calculation of the electronic structure. Finally, the *ab initio* molecular dynamics (AIMD) simulations are performed in the canonical (NVT) ensemble with the Nosé thermostat.

3. Results and discussion

3.1. Crystal structure

Using the method described above, a new silicon allotrope structure named *c*-Si16 was uncovered, as shown in Fig. 1. Figure 1a depicts the primitive cell of the crystal structure *c*-Si16, and Fig. 1b indicates that the structure is composed of Si tetrahedral units. Figure 1c shows a view from the *a*-axis.

TABLE I

Density, elastic constant, bulk elastic modulus B, shear modulus G, Young's modulus E, Poisson's ratio ν, and B/G ratio of c-Si16 along with those parameters of other silicon allotropes at ambient pressure.

Structure	c-Si16	Si-I[a]	h-Si_6[b]	t-Si_{64}[c]	$hP12$-Si[d]
ρ [g/cm^3]	2.16	2.40	1.71	1.662	2.51
C_{11} [GPa]	87	161	83	88	166
C_{12} [GPa]	58	62	34	20	66
C_{13} [GPa]	58	62	37	30	66
C_{22} [GPa]	87	161	83	88	166
C_{23} [GPa]	58	62	37	30	94
C_{33} [GPa]	87	161	157	95	148
C_{44} [GPa]	64	76	24	27	51
C_{55} [GPa]	64	76	24	27	51
C_{66} [GPa]	64	76	–	6	56
B [GPa]	68	95	58	48	94
G [GPa]	35	64	33	21	51
E [GPa]	90	157	83	55	129
ν	0.28	0.22	0.26	0.31	0.27
B/G	1.943	1.484	1.756	2.286	1.843

[a]Ref [28], [b]Ref [45], [c]Ref [46], [d]Ref [28]

Figure 1d shows the observation view of the structure along the [111] direction. It can be seen that there is a 3-fold rotation axis along the [111] direction. The c-Si16 belonging to the P-43m (No. 215) space group has the symmetry of the cubic crystal system and contains 16 silicon atoms in a conventional unit cell. For c-Si16, 16 Si atoms occupy an equivalent Wyckoff position of 16d (0.37500, 0.37500, −0.37500). At ambient pressure, the lattice parameters of the structure-optimized GGA level are a = 7.015 Å, b = 7.015 Å, and c = 7.015 Å. Usually, silicon composed of 4-coordinated atoms is more stable under normal pressure. The atoms in c-Si16 are all 6-coordinated. Therefore, the structure has a relatively high energy value compared to the Si-I. The Si–Si bond length in c-Si16 is 2.48 Å, which is slightly larger than that of the Si-I phase (2.35 Å). Due to the tetrahedral gap, c-Si16 has a smaller density (2.16 g/cm^3), while the density of the Si-I phase of the cubic diamond structure is 2.33 g/cm^3.

3.2. Mechanical and dynamic stability

The mechanical and dynamic stability of c-Si16 is demonstrated by calculating the elastic constant, bulk elastic modulus, shear modulus, Young's modulus, B/G, ν, and phonon spectrum of c-Si16. Through the stress–strain relation, we obtained the elastic constant of c-Si16. Since the c-Si16 structure belongs to the cubic crystal system, it has the simplest elastic matrix with only three independent elastic constants: C_{11}, C_{12}, and C_{44}. At 0 GPa, the precondition of stability for the cubic structure is that its elastic constant satisfies the Born mechanical stability criterion as shown below [42]

$$C_{11} - C_{12} > 0, \tag{1}$$

$$C_{11} + 2C_{12} > 0, \tag{2}$$

$$C_{44} > 0. \tag{3}$$

The elastic constants of c-Si16 are listed in Table I and are C_{11} = 87 GPa, C_{12} = 58 GPa, C_{44} = 64 GPa (see also [28, 45, 46]). Obviously, the three independent elastic constants of the structure satisfy the generic Born stability criteria of the cubic crystal system above, which means that the structure is mechanically stable.

When the atoms inside the crystal are arranged in different orientations, with different periods and degrees of density, the crystal will show disparate physical and chemical properties for different directions. It is feasible and effective to depict the anisotropy of crystal elasticity using Young's modulus diagram of a three-dimensional surface representation of a crystal. The variation of Young's modulus of cubic crystal system in any direction can be described by the following formula [43]

$$E^{-1} = S_{11} - 2\left(S_{11} - S_{12} - \frac{S_{44}}{2}\right)\left(l_1^2 l_2^2 + l_2^2 l_3^2 + l_1^2 l_3^2\right), \tag{4}$$

where l_1, l_2, and l_3 are the direction cosines of the tensile stress, and S_{ij} are the elastic compliance coefficients. By utilizing the formula (4), the three-dimensional surface representation of Young's modulus of c-Si16 in space is well elucidated, as shown in Fig. 2a. The two-dimensional projection of Young's modulus on the x–y plane is also illustrated for greater clarity in Fig. 2b. If the ratio of Young's modulus maximum to minimum ($E_{\max}/E_{\min}$) is equal to 1.0, the structure will appear isotropic; otherwise, it can be regarded as anisotropic. The $E_{\max}/E_{\min}$ value of c-Si16 is 3.7. This value is far from 1.0, which means the anisotropy of this structure is high.

According to the Voigt–Reuss–Hill (VRH) approximation [44], the bulk modulus (B [GPa]) and shear modulus (G [GPa]) of the c-Si16 were evaluated from the values of calculated elastic constants; the results are shown in Table I. It is worth noting that, compared to the other silicon allotropes listed in Table I, c-Si16 has a relatively larger shear modulus (35 GPa) and a larger bulk modulus (68 GPa). Young's modulus (E [GPa]) and Poisson's ratio (ν) can be calculated from the values of the bulk and shear moduli according to the following expressions

$$E = \frac{9BG}{3B + G} \tag{5}$$

and

$$v = \frac{3B - 2G}{2\,(3B + G)}. \tag{6}$$

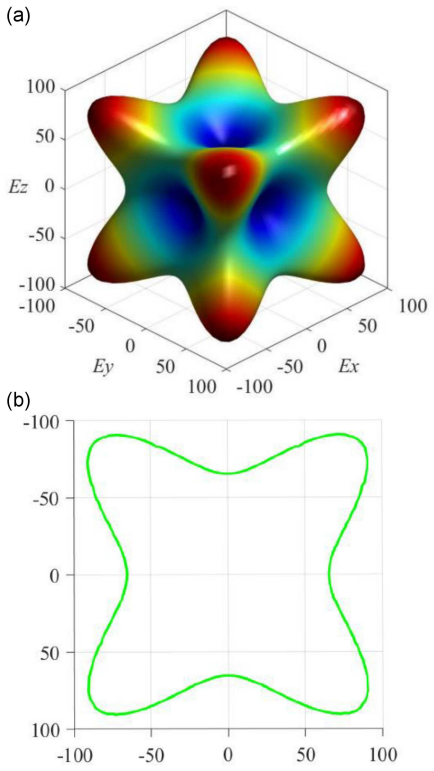

Fig. 2. The three-dimensional surface representation of the Young's modulus (a) and two-dimensional representation of Young's modulus in the x–y plane (b) for c-Si16.

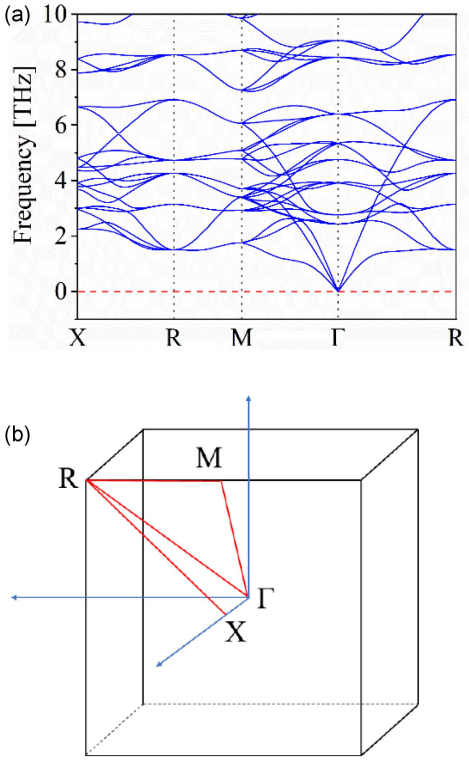

Fig. 3. (a) Calculated phonon dispersion curve of c-Si16. (b) High symmetry points paths for phonon dispersion.

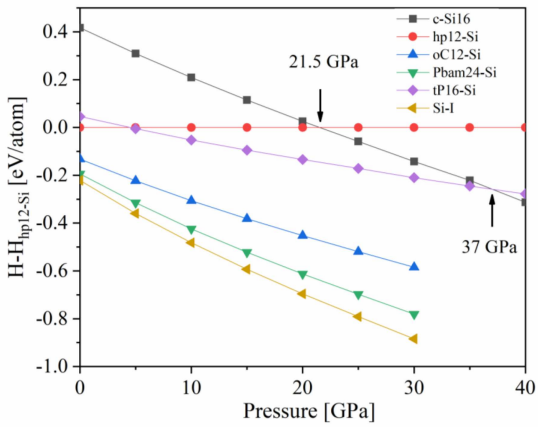

Fig. 4. Calculated enthalpies of different silicon structures relative to the hp12-Si as a function of pressure.

The moduli of Si-I, h-Si$_6$, t-Si$_{64}$, and hP12-Si are also listed in Table I for comparison. Both bulk elastic modulus and shear modulus of c-Si16 are larger than the corresponding quantities of t-Si$_{64}$ structure, whereas these quantities of c-Si16 structure are smaller than those of Si-I, indicating that its mechanical stiffness is between those of t-Si$_{64}$ and Si-I structures. In terms of measuring the brittleness and ductility of the crystal structure, the ratio of B/G can be an effective method. Crystals exhibit ductility if the B/G ratio is greater than 1.75; if it is not, on the contrary, it means that the crystal has a certain brittleness. For c-Si16, the ratio of B/G is 1.913, indicating its ductility. The dynamic stability of c-Si16 is confirmed by the phonon spectrum, as shown in Fig. 3. The fact that there is no imaginary frequency in the entire Brillouin zone indicates the dynamic stability of the c-Si16. In summary, under ambient pressure, the silicon allotrope of the c-Si16 structure is stable.

3.3. Thermodynamic stability

To examine the thermodynamic stability of the c-Si16 structure, the enthalpy of the proposed structure was compared with the corresponding enthalpy of experimentally known Si-I as well as other proposed stable silicon phases (oC12-Si, tP16-Si, hP12-Si [21], *Pbam*-Si24 [47]), as shown in Fig. 4. As the pressure increases, the enthalpy difference between c-Si16 and hp12-Si decreases. The enthalpy of c-Si16 becomes lower than that of hp12-Si and that of tp16-Si above 21.5 and 37 GPa, respectively. The AIMD simulations were calculated for 6 ps at 300 K and 500 K and depicted in Fig. 5. The total energy of the supercell for c-Si16 gradually fluctuates at a stable level, implying that c-Si16 can be stable up to at least 500 K.

3.4. Electronic properties

Under ambient pressure, silicon atoms usually form covalent bonds by sp^3 hybridization, but because the valence electrons are limited to covalent bands, very few electrons are free to move around in an atom. Although the high-pressure phase metallic allotropes of silicon are widespread, there are few metallic silicon allotropes that have a stable state under ambient pressure. The electronic band structure and partial density of states (PDOS) of *c*-Si16 were plotted with data obtained from VASP calculations, as shown respectively in Fig. 6 and Fig. 7. From the fact that the energy bands cross the Fermi level (E_F) indicated by the dotted line, we can conclude that *c*-Si16 has a certain metallicity. As shown in Fig. 7, in the partial-wave density of states (DOS) diagram of electrons, there is a partial-wave DOS that crosses the Fermi level, which also confirms the metallic characteristics of the *c*-Si16 system. It can also be concluded from Fig. 7 that the conductivity of *c*-Si16 mainly comes from the *p*-orbital electrons of silicon.

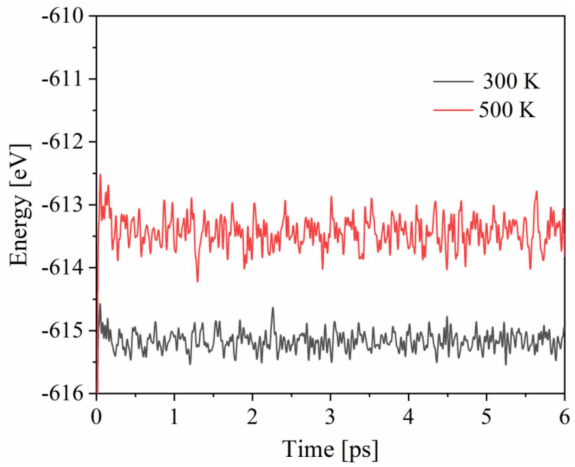

Fig. 5. AIMD at 300 K and 500 K for *c*-Si16.

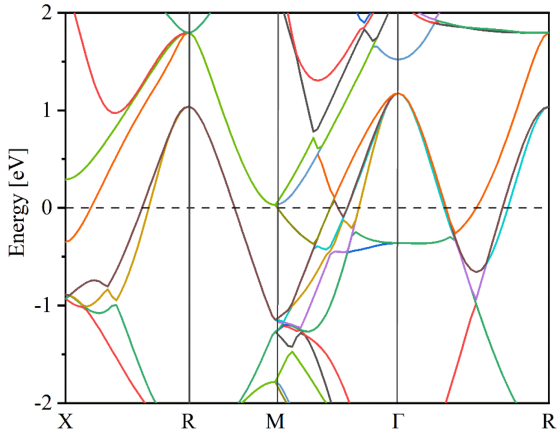

Fig. 6. Electronic band structure for *c*-Si16 at the PBE level.

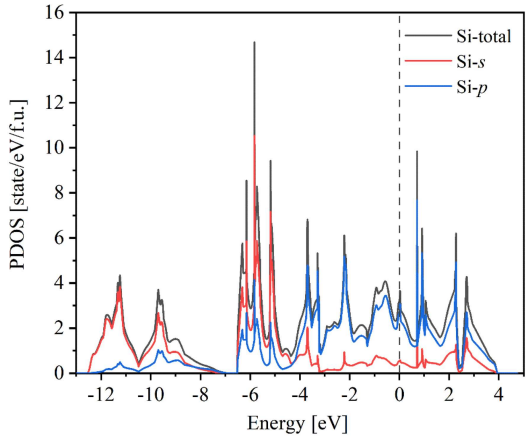

Fig. 7. Partial density of states; position of the dotted line represents the Fermi level.

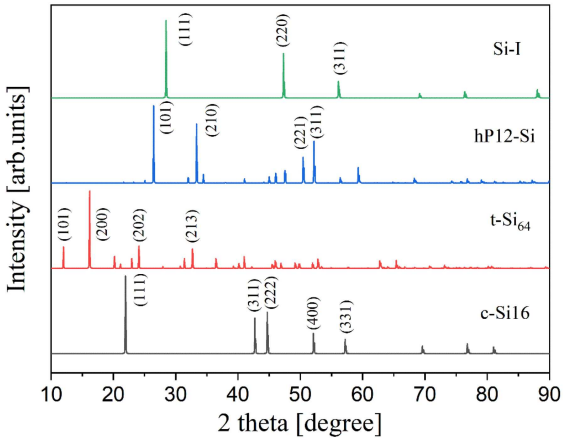

Fig. 8. XRD of *c*-Si16 and three other common silicon allotropes. The X-ray wavelength is 1.5406 Å with a copper source.

In addition, through the analysis of Fig. 7, it can be concluded that the density of states of *c*-Si16 has the following two characteristics: First, the density of states of each peak in the low energy region (−12 eV−−5 eV) mainly comes from the contribution of *s*-orbital electrons in silicon atoms, while the contribution of *p*-orbital to the density of states is very small. Secondly, the density of states of each peak in the low energy region (−4 eV–0 eV) and the high energy region (0–4 eV) mainly comes from the contribution of *p*-orbital electrons in silicon atoms, while the contribution of *s*-orbital to the density of states is very small.

In order to facilitate the possible experimental observation and research on the structure of *c*-Si16 in the future, we provide more information and characteristics by calculating the X-ray diffraction (XRD) pattern of *c*-Si16, which is plotted in Fig. 8. The calculations used X-rays with a wavelength of 1.5406 Å. The calculated XRD patterns of Si-I, *t*-Si_{64}, and *hP*12-Si are also plotted for comparison.

The first strongest peak (111) is located around 21.9°, and the four other characteristic peaks at $2\theta \approx 42.7°$, 44.8°, 52.2°, and 57.2° correspond to the crystal planes of (311), (222), (400), and (331), respectively. Besides these main diffraction peaks, there are also several other small peaks. The main characteristic peaks of the structure listed above will contribute to the phase identification of *c*-Si16 in possible future experiments.

4. Conclusions

Utilizing the structure prediction program of the particle swarm optimization algorithm combined with the first-principles calculation method, we have first discovered a new metallic silicon allotrope, i.e., *c*-Si16. We studied the structural properties, mechanical properties, and electronic properties of *c*-Si16 using first-principles calculations. The mechanical stability and dynamic stability are demonstrated by the calculation of elastic constants and phonon spectra at 0 GPa. According to the characteristics of $B/G > 1.75$, it can be determined that *c*-Si16 is a ductile material. It also can be seen from the three-dimensional surface representation of Young's modulus and the projection of Young's modulus on the x–y plane that the structure exhibits relatively large anisotropy. Concerning electronic properties, *c*-Si16 exhibits some metallic properties, and the presence of this metallicity is largely due to the contribution of the *p*-orbital of silicon.

Acknowledgments

This work was financially supported by the National Natural Science Foundation of China (Grant Nos. 11965005 and 11964026), the Natural Science Basic Research Plan in Shaanxi Province of China (Grant Nos. 2023-JC-YB-021, 2022JM-035), the Fundamental Research Funds for the Central Universities, and the 111 Project (B17035). All the authors thank the computing facilities at the High Performance Computing Center of Xidian University.

References

[1] J.S. Kilby, *IEEE Solid-State Circuits Soc. Newsl.*, **12**, 44 (2007).

[2] R.N. Noyce, *IEEE Solid-State Circuits Soc. Newsl.*, **12**, 34 (2007).

[3] D.E. Carlson, C.R. Wronski, *Appl. Phys. Lett.* **28**, 671 (1976).

[4] M.A. Green, *Solar Cells: Operating Principles, Technology, and System Applications*, Englewood Cliffs, 1982.

[5] L. Fan, D. Yang, D. Li, *Materials* **14**, 3964 (2021).

[6] J.C. Jamieson, *Science* **139**, 762 (1963).

[7] M.I. McMahon, R.J. Nelmes, *Phys. Rev. B.* **47**, 8337 (1993).

[8] H. Olijnyk, S.K. Sikka, W.B. Holzapfel, *Phys. Lett. A.* **103**, 137 (1984).

[9] M. Hanfland, U. Schwarz, K. Syassen, K. Takemura, *Phys. Rev. Lett.* **82**, 1197 (1999).

[10] S.J. Duclos, Y.K. Vohra, A.L. Ruoff, *Phys. Rev. Lett.* **58**, 775 (1987).

[11] S. Wippermann, Y. He, M. Vörös, G. Galli, *Appl. Phys. Rev.* **3**, 040807 (2016).

[12] J.-T. Wang, C. Chen, H. Mizuseki, Y. Kawazoe, *Phys. Rev. Lett.* **110**, 165503 (2013).

[13] R.H. Wentorf Jr, J.S. Kasper, *Science* **139**, 338 (1963).

[14] J. Crain, G.J. Ackland, J.R. Maclean, R.O. Piltz, P.D. Hatton, G.S. Pawley, *Phys. Rev. B.* **50**, 13043 (1994).

[15] M.A. Zwijnenburg, K.E. Jelfs, S.T. Bromley, *Phys. Chem. Chem. Phys.* **12**, 8505 (2010).

[16] S. Botti, J.A. Flores-Livas, M. Amsler, S. Goedecker, M.A. Marques, *Phys. Rev. B.* **86**, 121204 (2012).

[17] Z. Zhao, F. Tian, X. Dong, Q. Li, Q. Wang, H. Wang, X. Zhong, B. Xu, D. Yu, J. He, H. Wang, Y. Ma, Y. Tian, *J. Am. Chem. Soc.* **134**, 12362 (2012).

[18] H.-Y. Zhao, J. Wang, Q.-M. Ma, Y. Liu, *Phys. Chem. Chem. Phys.* **15**, 17619 (2013).

[19] B.D. Malone, M.L. Cohen, *Phys. Rev. B.* **85**, 024116 (2012).

[20] H.J. Xiang, B. Huang, E. Kan, S.-H. Wei, X.G. Gong, *Phys. Rev. Lett.* **110**, 118702 (2013).

[21] Q. Wang, B. Xu, J. Sun, H. Liu, Z. Zhao, D. Yu, C. Fan, J. He, *J. Am. Chem. Soc.* **136**, 9826 (2014).

[22] A. Bautista-Hernández, T. Rangel, A.H. Romero, G.-M. Rignanese, M. Salazar-Villanueva1, E. Chigo-Anota, *J. Appl. Phys.* **113**, 193504 (2013).

[23] Y. Fujimoto, T. Koretsune, S. Saito, T. Miyake, A. Oshiyama, *New J. Phys.* **10**, 083001 (2008).

[24] F. Wu, D. Jun, E. Kan, Z. Li, *Solid State Commun.* **151**, 1228 (2011).

[25] B.D. Malone, J.D. Sau, M.L. Cohen, *Phys. Rev. B* **78**, 035210 (2008).

[26] Q. Fan, C. Chai, Q. Wei, H. Yan, Y. Zhao, Y. Yang, X. Yu, Y. Liu, M. Xing, J. Zhang, R. Yao, *J. Appl. Phys.* **118**, 185704 (2015).

[27] K. Luo, Z. Zhao, M. Ma, S. Zhang, X. Yuan, G. Gao, X. Zhou, J. He, D. Yu, Z. Liu, B. Xu, Y. Tian, *Chem. Mater.* **28**, 6441 (2016).

[28] L. Sun, K. Luo, B. Liu, Q. Han, X. Wang, Z. Liang, Z. Zhao, *Chin. J. High Pressure Phys.* **33**, 020103 (2019).

[29] Q. Wang, K. Luo, M. Ma, D. Yu, J. He, *Chi. Sci. Bull.* **60**, 2616 (2015).

[30] H.-J. Sung, W.H. Han, I.-H. Lee, K.J. Chang, *Phys. Rev. Lett.* **120**, 157001 (2018).

[31] Z. Wen, G. Lu, S. Mao, H. Kim, S. Cui, K. Yu, X. Huang, P.T. Hurley, O. Mao, J. Chen, *Electrochem. Commun.* **29**, 67 (2013).

[32] Y. Wang, J. Lv, L. Zhu, Y. Ma, *Phys. Rev. B* **82**, 094116 (2010).

[33] Y. Wang, J. Lv, L. Zhu, Y. Ma, *Comput. Phys. Commun.* **183**, 2063 (2012).

[34] Q. Wei, Y. Yan, X. Jia, H. Yan, M. Zhang, Z. Wu, Y. Zhou, *Phys. Lett A* **457**, 128540 (2023).

[35] G. Wang, Z. Ma, J.-W. Jiang, J. Yang, Y.-L. Sun, Z.-F. Qian, P. Huang, P. Zhang, S.-H. Wei, *Phys. Rev. Appl.* **19**, 034014(2023).

[36] Y. Liu, T. Cui, D. Li, *IScience* **26**, 106113(2023).

[37] M. Li, M. Zhang, P. Zhang, S. Zhang, D. Liu, Y. Zhao, J. Zhang, *J. Alloys Compd.* **933**, 167818 (2023).

[38] G. Kresse, J. Furthmüller, *Phys. Rev. B* **54**, 11169 (1996).

[39] J.P. Perdew, K. Burke, M. Ernzerhof, *Phys. Rev. Lett.* **77**, 3865 (1996).

[40] W. Kohn, L.J. Sham, *Phys. Rev.* **140**, A1133 (1965).

[41] A. Togo, F. Oba, I. Tanaka, *Phys. Rev. B* **78**, 134106 (2008).

[42] F. Mouhat, F.-X. Coudert, *Phys. Rev. B* **90**, 224104 (2014).

[43] J.F. Nye, *Physical Properties of Crystals: Their Representation by Tensors and Matrices*, Oxford University Press, 1985.

[44] R. Hill, *Proc. Phys. Soc. A* **65**, 349 (1952).

[45] Y. Guo, Q. Wang, Y. Kawazoe, P. Jena, *Sci Rep.* **5**, 1 (2015).

[46] Q. Fan, R. Niu, W. Zhang, W. Wang, Y. Ding, S. Yun, *ChemPhysChem* **20**, 128 (2019).

[47] A. Mujica, C.J. Pickard, R.J. Needs, *Phys. Rev. B* **91**, 214104 (2015).